View metadata, citation and similar papers at core.ac.uk

brought to you by CORE

provided by Queensland University of Technology ePrints Archive

QUT Digital Repository:
http://eprints.qut.edu.au/

Situ, Rong and Yang, William and Tu, Jiyuan and Yeoh, Guan H. and Hibiki, Takashi and Ishii, Mamoru and Park, G. C. and Brown, Richard J. (2008) Flow Visualazation Of Bubble Condensation In Forced Convective Subcooled Boiling Flow. In Prenel, Jean Pierre and Bailly, Yannick and Champoussin, Jean Claude, Eds. *Proceedings ISFV13 - 13th International Symposium on Flow Visualization; FLUVISU12 - 12th French Congress on Visualization in Fluid Mechanics*, Nice, France.

© Copyright 2008 The authors

ISFV13 - 13th International Symposium on Flow Visualization
FLUVISU12 - 12th French Congress on Visualization in Fluid Mechanics
July 1-4, 2008, Nice, France

FLOW VISUALAZATION OF BUBBLE CONDENSATION IN FORCED CONVECTIVE SUBCOOLED BOILING FLOW

R. Situ[1], W. Yang[2], J.Y. Tu[3], G. H. Yeoh[4], T. Hibiki[5], M. Ishii[5], G. C. Park[6], R. J. Brown[1]
1. School of Engineering Systems, Queensland University of Technology, GPO Box 2434, Brisbane, Queensland 4000, Australia
2. CSIRO Light Metals Flagship, Box 312, Clayton South, VIC 3169, Australia.
3. SAMME, RMIT University, PO Box 71, Bundoora, Victoria 3083, Australia.
4. Australian Nuclear Science Technology Organization, PMB 1, Menai, NSW 2234, Australia.
5. School of Nuclear Engineering, Purdue University, West Lafayette, IN 47907-2017, USA.
6. Dept. Nuclear Engineering, Seoul National University, Seoul, 151-742 Korea.

KEYWORDS:
Main subject(s): *Bubble Condensation, Subcooled boiling Flow,*
Fluid: *Water,*
Visualization method(s): *Particle/Droplet Image Analysis*

***ABSTRACT** : Subcooled boiling bubble condensation experiments were conducted in a vertical-upward annular channel by using water as the testing fluid at atmosphere pressure. The test runs comprised of bulk liquid temperatures, velocities and wall heat fluxes ranging from 75.0℃ to 98.0℃, 0.25 m/s to 1.0 m/s and 150 kW/m^2 to 200 kW/m^2 respectively. A particle/droplet image analysis system was employed to capture the flow channel at four locations downstream of heated section for a total of 13 test conditions. The bubble Sauter-mean diameter was obtained in the range of 0.1 mm to 0.9 mm. It is also found that bubble sizes increase with the increase of liquid temperature or the decrease of liquid velocity. The condensation Nusselt number was calculated to be in the range of 10^{-4} to 10^{-1}, which is much smaller than the typical range of 10^{0} to10^{2}. This might due to the existence of non-condensable gas in the bubble.*

1 Introduction

Many industrial applications, for instance, boiler, boiling water reactor, and the new generation of electronic and computer system, are seriously interested in the understanding and modeling of subcooled boiling flow. The mere existence of thermodynamic non-equilibrium between the gas and liquid phases greatly complicates the analysis of subcooled boiling flows in the core (bulk flow) region. Various two-phase flow models have been proposed to deal with the discontinuity at the interfaces between the different phases. For example, some measured success has been achieved by the homogeneous and drift-flux models in some engineering applications. However, intrinsic limitations preclude these models from robustly handling two-phase flows that are either transient or in a complex geometry. An alternative approach, based on solving a set of conservative equations for each phase proposed in the two-fluid model, provides a feasible solution to these complex problems [1]. Provided that suitable boundary and initial conditions are imposed, the spatial and temporal distribution of each phase can be adequately simulated. The weakest link of the two-fluid model is, however, the modelling of the phase interaction terms that couple the transfer of mass, momentum, and energy across the interface. These phase interaction terms are specifically related to the interfacial area concentration, since all the interfacial transfer occurs through the liquid-gas interface.

A successful simulation of the subcooled boiling flow in the core region should precisely describe two basic geometric parameters: (i) void fraction (defined as the fraction of gas phase in the mixture), and (ii) interfacial area concentration (defined as the total interfacial area, or bubble surface area, divided by the mixture volume). These two parameters can be mathematically accommodated by adopting the two-fluid model and either the Interfacial Area Transport Equation (IATE) or the Multiple-Size Group (MUSIG) model. These two models both adopt a population balance approach to model the source and sink terms of interfacial area concentration or bubble number due to bubble coalescence, break-up, nucleation, condensation, and other mechanisms associated with heat and mass transfer processes involved in subcooled boiling flow.

In previous research by the authors, all the source terms in the IATE have been thoroughly investigated. The source and sink terms due to bubble coalescence and break-up has been successfully modeled for isothermal flows [2-5]. Additionally, a bubble-layer thickness model was developed to avoid covariance in cross-sectional averaging of the IATE in subcooled boiling flows [6]. As one of the most important source term, the bubble nucleation on heater surface consists of three contributing parameters, i.e., active nucleation site density, bubble lift-off diameter, and bubble departure frequency. Recently, Hibiki and Ishii [7] mechanistically modeled the active nucleate site density by accounting for the distribution of the critical cavity size and contact angle of the bubble on the heated surface. This model was correlated by taking into consideration various active nucleation site density data taken in pool boiling and convective flow boiling systems. Situ et al. [8-10] conducted on a range of photographic studies of subcooled boiling flows to investigate the bubble departure and lift-off. The model of bubble lift-off size has been developed based on the force balance analysis of a lifting-off bubble. Besides, a correlation of bubble departure frequency was proposed and it agrees well with the existing datasets available in literature.

Another important source/sink term in the IATE is the sink term due to bubble condensation. It has been extensively studied in pool boiling and flow boiling, which has been thoroughly reviewed by Zeitoun et al. [11], and later updated by Warrier et al. [12] and Park, et al. [13]. The bubble condensation experiments were mostly performed to study stagnant bubbles in a pool [14-16]; or to study moving bubble in a stagnant liquid [17-19]; or to study bubbles collapsing in a flow boiling[11, 12]. Most of the studies classified the bubble condensation into heat transfer or inertial controlled condensation. Some researcher [20] found that inertial controlled condensation occurs at high liquid subcooling, while heat transfer controlled condensation happens at relative low subcooling. Chen and Maying [19] obtained the criteria to be at $Ja > 100$ (for fully inertial controlled) and $Ja < 80$ (for complete heat transfer controlled). On the other hand, Park et al. [13] divided a whole condensation process of a bubble, generated from the heated surface, into two stages: (i) heat transfer controlled region, starting from maximum bubble size, condensing in low surrounding subcooling, and finishing when bubble is reduced to 0.4 of maximum size, and rapid decreasing rate occurs; (ii) inertial controlled region, where bubble collapses sharply a critical collapsing bubble diameter Dc which is around 25 μm at atmosphere pressure. By analyzing these two regions, a bubble condensation sink term in the IATE was developed [13]. Due to the limitation of measuring technique, most of the experiments have been conducted by measuring the size of one or a few bubbles, and the bubble size distribution and the averaged bubble size cannot be captured. In addition, the low resolution setup of the camera makes it difficult to obtain bubble in micrometer level (less than 0.1 mm).

The purpose of this paper is to investigate bubble condensation phenomena at micrometer range in subcooled boiling flow. To this end it will utilize the recently-developed Particle/Droplet Image

Analysis (PDIA) technique to obtain bubble size and velocity distributions, compare the data with existing correlations, and propose new models.

2 Experimental Setup

2.1 Test Facility

An experimental facility has been designed to measure the relevant two-phase parameters necessary for developing constitutive models for the two-fluid model in subcooled boiling flow. The experimental facility is a scaled-down loop from a prototypic boiling water reactor based on proper scaling criteria for geometric, hydrodynamic, and thermal similarities [21, 22]. The schematic diagram of the flow loop is shown in Figure 1. The pre-degassed distilled water is held in the main tank. The main tank has a 2kW heater to maintain the temperature. The water is pumped by a Lowara centrifugal pump and divided into four separate lines. Each line runs to a fitting that is connected to the bottom of the test section. The test section is an annulus formed by a clear polycarbonate tube on the outside with an ID of 38.1 mm, and a cartridge heater on the inside with an OD of 19.1 mm. Thus, the hydraulic equivalent diameter, D_H, is 19.1 mm. The test section has an overall length of 1200 mm with a heated section of 200 mm in length. The maximum heat flux of the heater is 200 kW/m^2. An image box (60 cm length) was installed on the test section to minimize the image distortion. The image box was filled with glycerin because its index of refraction (1.473) is close to that of polycarbonate tube (1.58). On the top of the test section, an expansion joint is installed to accommodate the thermal expansion of the polycarbonate test section. A separation tank is used to separate vapor phase from water. The steam is then condensed, and the water is returned to the main tank. The separation tank is located directly above the main tank.

2.2 Particle/Droplet Image Analysis (PDIA) System

Particle/Droplet Image Analysis (PDIA) is a newly developed digital image analysis technique by Oxford Lasers, which is capable of determining the properties of individual bubbles or droplets such as their velocity, size, shape and concentration over a finite region of interest in the flow. The principle of PDIA technique is to use an automated segmentation threshold algorithm for the quantitative analysis of bubble or droplet images [23]. This method is based on the original approach adopted by Yule et al. [24], using the degree of image focus determined from the edge gradient intensity of a bubble or droplet image.

It is possible to determine the diameter of a droplet from an estimate of the pixel area of a shadow droplet image by using a simple threshold algorithm, and thus simultaneous estimates of the droplet size and sphericity can be obtained. However, out-of-focus droplets appear typically up to 30% larger than they are. The PDIA technique uses two thresholds, one to measure the grey, out-of-focus border, and the other to measure the dark core. From the ratio of these areas, the true droplet size and its distance from the plane of best focus can be deduced. Moreover, the PDIA software also corrects the bias introduced by droplets that touch the edges of the image: large droplets are more likely to touch the edges [25].

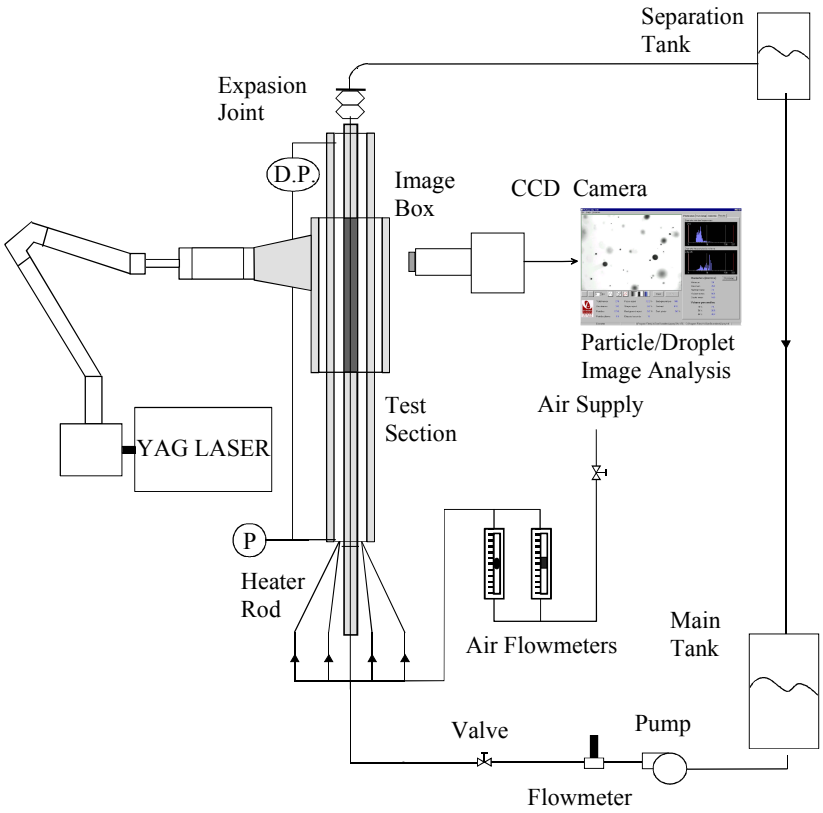

Fig. 1. Experimental facility.

Diameter measurement in PDIA is based on an area estimate of the shadow image of an individual droplet, and is straightforward for a perfect sphere. As reported by Whybrew et al. [23], the image analysis technique also permits the sizing of non-spherical droplets where the diameter for a droplet of arbitrary shape, D_a, is based on the equivalent circular area as given by equation (1):

$$D_a = C\sqrt{\frac{4A}{\pi}}, \tag{1}$$

where A is the total number of pixels and C is the ratio of microns to pixel obtained from calibration. The droplet based on the equivalent circular perimeter, D_p is defined through the ratio of microns to pixels, C, and the is the number of pixels on the perimeter of the non-spherical droplet, P, defined in equation (2).

$$D_p = \frac{CP}{\pi}, \tag{2}$$

Figure 1 shows a schematic diagram of the PDIA apparatus used in the current study. A double-pulsed Nd: YAG laser was used as the illumination source with pulse duration of 5 ns. The fluorescent diffuser coupled with an articulated beam delivery arm produces an expanding cone of light with a uniform background intensity distribution. Image acquisition was achieved with a non-intensified 12-bit CCD camera (PCO Sensicam) with a 1280 × 1024 pixel array and pixel dimensions of 6.7 × 6.7 μm. An Oxford Lasers long distance microscope lens (Model Option 4) provided a magnification of 0.64

offering a resolution of approximately 11.55 μm/pixel (after calibration considering the image distortion effect of test tube). It was found that 400 continual images at the rate of four frames per second were needed to get stable statistical mean diameter of the bubbles for each experimental operating condition. In addition a background image was also taken without the presence of bubbles. Due to the complex structure of the annual test section causing highly non-uniform image illumination, a Background Subtraction Mode within the PDIA VisiSize Solo software (version 2.089) was employed.

2.3 Experimental Procedure

The experiments were conducted rigorously. In preparing for an experiment, the distilled water in the main tank is degassed by heating up the tank for 24 hours. Before the measurement, the flow reaches steady state, and the inlet temperature and fluid velocity keep constant for 30 minutes. Experiments of 13 conditions, as shown in Table 1, were performed for the investigation of bubble condensation downstream of the heated section. For each condition, the camera were placed at four locations in the unheated section, i.e., 0 mm (or 20 mm), 50 mm, 100mm, and 200mm. The temperature at the end of heated section ranges from 75.0 to 98.0 °C; the inlet velocity varies from 0.25 to 1.0 m/s; and the heat flux changes from 150 to 200 kW/m^2. In all experiments, the temperatures at several locations (test section inlet, outlet, and heated section end) were measured by the thermocouple with accuracy of ±0.1 °C. Besides, the pressures at inlet and outlet of the test section were also measured by Gems Sensors 2200 series pressure transducers. In addition, heat flux and inlet velocity are acquired by a data acquisition system. The measurement accuracies of heat flux, liquid temperature, liquid velocity, and pressure are ±1%, ±1.5°C, ±1.5% of reading, ±25%, respectively.

Table 1. Experimental conditions.

Test	T_{in} [°C]	T_{out} [°C]	q''_w [kW/m^2]	v_{fin} [m/s]	p_{in} (kPa)	p_{out} (kPa)
1	88.9	89.8	146.6	0.498	15.8	2.4
2	96.5	98.2	148.4	0.501	15.1	2.3
3	89.5	90.0	147.5	0.999	16.2	2.4
4	70.9	75.2	201.6	0.247	15.2	2.1
5	74.8	80.0	201.2	0.249	16.1	2.0
6	85.3	90.1	200.8	0.249	15.3	2.4
7	90.2	95.0	201.7	0.250	15.5	2.0
8	77.7	79.9	200.7	0.501	16.0	2.4
9	82.7	84.9	201.2	0.501	16.2	2.1
10	87.8	90.0	200.6	0.501	16.9	2.6
11	92.4	95.1	200.8	0.498	14.8	2.0
12	89.3	90.0	201.3	0.999	16.1	2.4
13	9.9	95.1	200.9	0.999	15.9	2.1

3 Results and Analysis

Data of bubble Sauter-mean diameter were extracted from pictures by using VisiSize Solo software from Oxford Lasers. For each experimental condition, a total of 200 or 400 pairs of image files were processed to ensure enough number of bubbles to be available for analysis. During the analyzing, data of bubble diameter was obtained by analyzing every first image of the pair of images. Since the image illumination was highly non-uniform, the reference background image was subtracted from the original image. Next, the adaptive mode of 55% was taken to obtain bubble images. After that, shape sphericity less than 0.2 were rejected. The shape sphericity is defined as

$$S = \frac{D_a}{D_p} = \sqrt{\frac{4\pi A}{P^2}}\,. \tag{3}$$

When diameters of all the bubbles were known, the averaged bubble diameter can be obtained by choosing different method. In order to better comparing with datasets in literature, the Sauter-mean method was chosen:

$$D_{sm} \equiv \sum_k D_k^3 \Big/ \sum_k D_k^2\,. \tag{4}$$

Averaged bubble Sauter-mean diameters at one axial location was obtained by setting the whole flow channel as the window; while radial distribution profile of the local bubble Sauter-mean diameter was obtained by setting the analysis window as 10% of the flow channel width (20% windows were chosen for Test 2, 7, 11, and 13 due to the appearance of large bubbles).

Another important output from the software is bubble velocity, which was obtained by particle tracking method which analyzing every pair of images. In the velocity mode, several parameters were set: bubble flow direction (upwards), maximum angle deviation (< 15°), and maximum pixel separation (determined according to liquid velocity). The mean bubble velocity was obtained by averaging all the bubbles in the window.

3.1 Bubble Sauter-mean diameter radial profile

Figure 1 shows the radial profile of bubble Sauter-mean diameter. Comparing with Test 1 and Test 2 in Fig. 1 finds that bubble diameter increases as the liquid temperature increases from 90 to 98°C. Similar phenomena can be found by comparing Test 4-7 and Test 8-11. In addition, bubble layer tends to expand to the core region, and big bubbles can be found (for unheated length z_u = 20mm). This suggests that bubble can survive at higher temperature. On the other hand, increase of liquid velocity seems to reduce the bubble size, which can be seen by comparing Test 1 and 3, Test 5 and 8, and Test 6 and 10, etc.

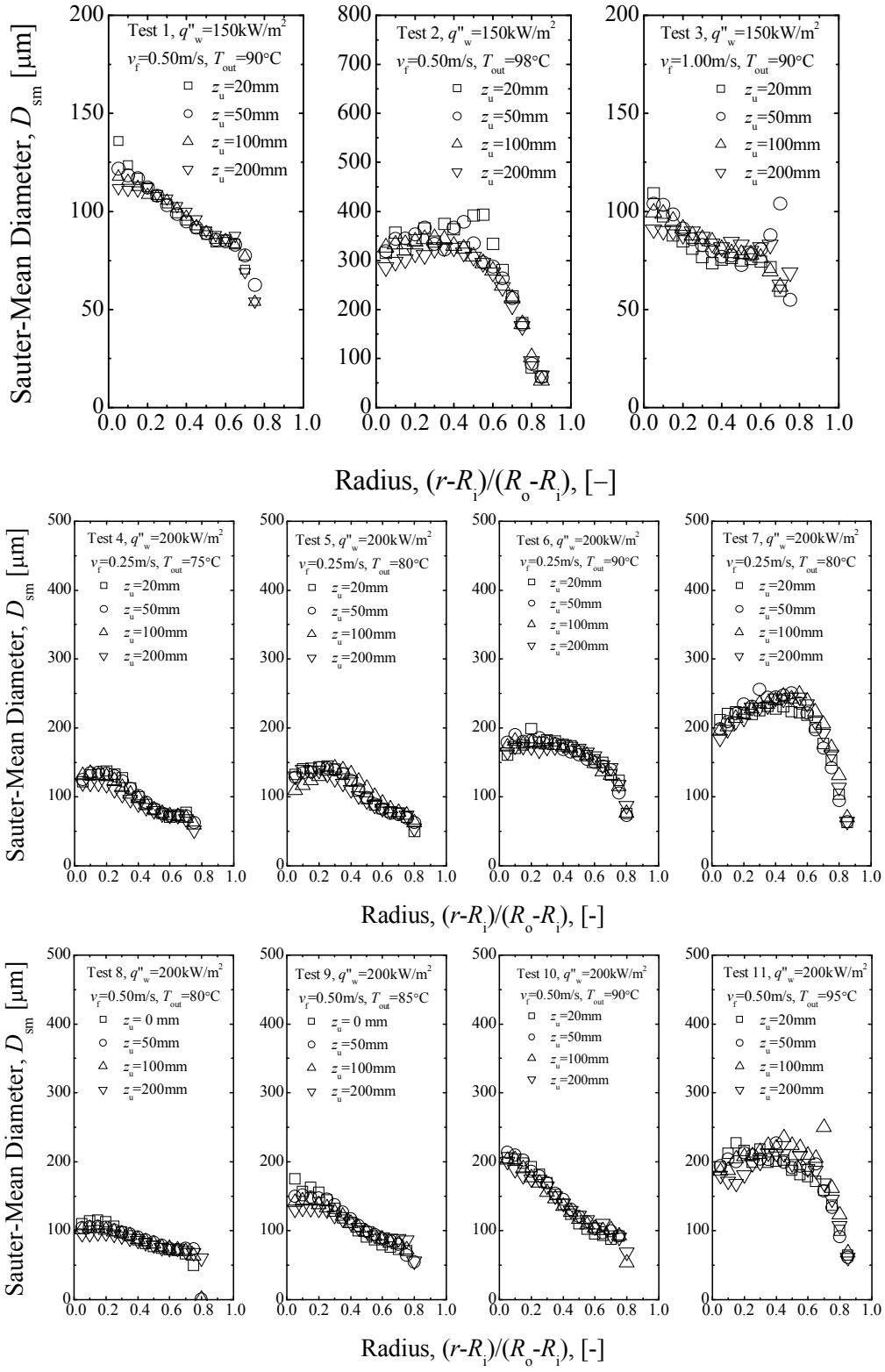

Fig. 2. Bubble Sauter-mean diameter radial profile.

3.2 Bubble velocity radial profile

Figure 3 shows the radial profile of bubble velocity, which agrees well with turbulent liquid velocity profile. Comparing with Test 1 and Test 3 finds that bubble velocity increase correspondingly with the increase of liquid velocity from 0.5 to 1.0 m/s. In addition, comparing with Test 1 and 2 find that the peak of velocity profile moves closer to left side, which is the heated surface. This can be explained with reference of Fig. 2(a), where bubble size is in the range of 300 to 400μm in Test 2 comparing with 100mm in Test 1. Thus the void fraction in Test 2 is much higher than in Test 1, which suggests that higher void fraction will result in higher bubble velocity. These phenomena can also be found in other subcooled boiling experiments [22]. Another interesting finding in test 2 is that bubble velocity decrease as the bubble travels in the unheated section, from z_u = 20mm to z_u = 200mm. This figure indicates that bubble diameter decrease in condensing flow, so does the bubble velocity.

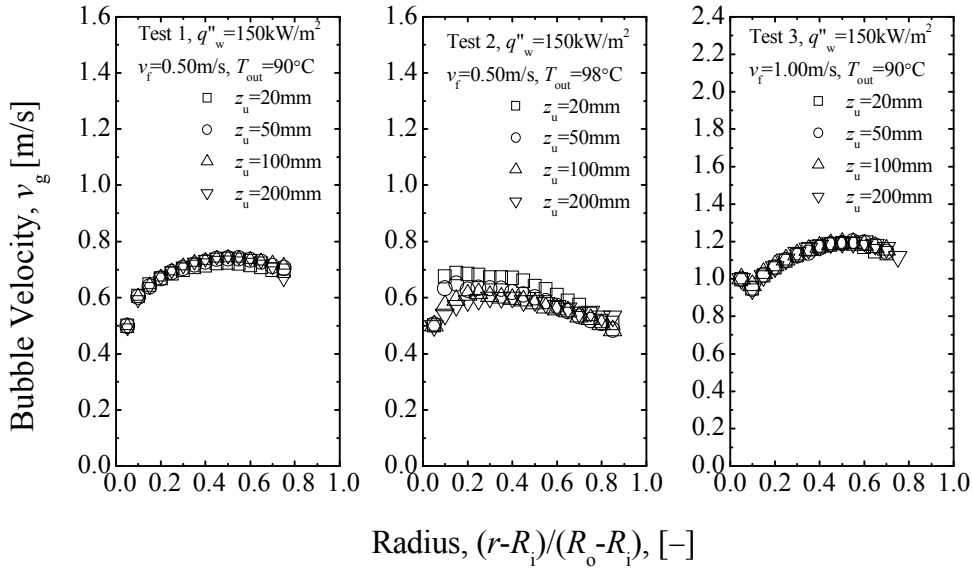

Fig. 3. Bubble velocity radial profile.

3.3 Bubble Sauter-mean diameter axial profile

Axial profiles of bubble Sauter-mean diameter are plotted in Fig. 4. It is suggested that bubbles collapse sharply when the bubble size is more than 400 μm, for conditions Test 2 and 11. However, after bubbles drop below 300 mm, bubbles condensation rate is reduced. The reducing of condensation rate can be explained clearly by drawing the condensation Nusselt number, which is defined as

$$Nu_c = -\frac{\rho_g i_{fg} D_{sm}}{2k_f\left(T_{sat}-T_f\right)}\frac{\mathrm{d}D_{sm}}{\mathrm{d}t}, \qquad (5)$$

where ρ_g, i_{fg}, k_f, T_{sat}, T_f are vapor density, latent heat, liquid thermal conductivity, saturation temperature, liquid temperature, respectively. Hence, the condensation Nusselt number is calculated from the experimental parameters, and plotted in Fig. 5 against Sauter-mean diameter and bubble Reynolds number

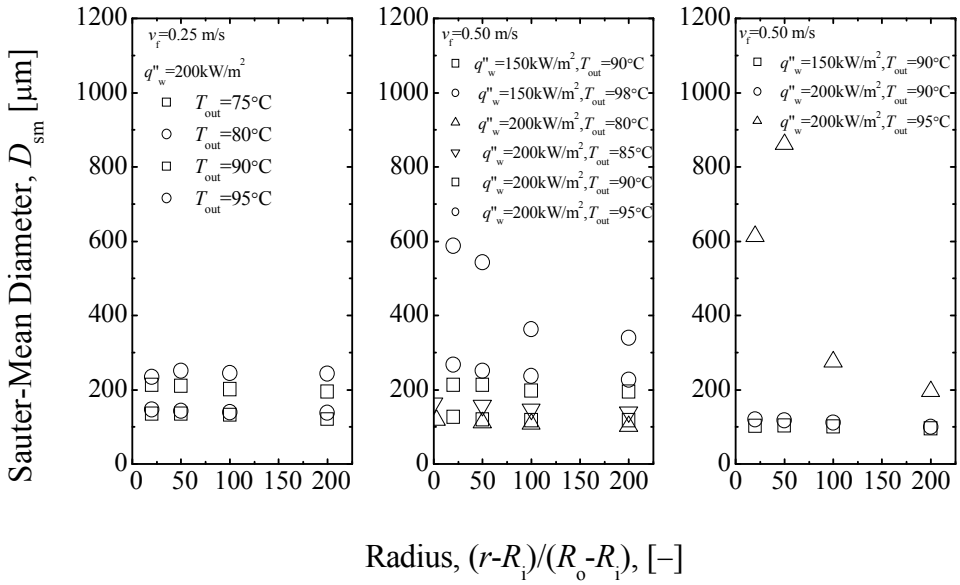

Fig. 4. Bubble Sauter-mean diameter axial profile.

$$Re_b = -\frac{\rho_f D_{sm}\left(v_g - v_f\right)}{\mu_f}, \tag{6}$$

where ρ_f, μ_f are liquid density and liquid viscosity. The existing models of condensation Nusselt number, described in Table 2, are compared. The results show that all the models predict Nu_c to be in the range of 1 to 10, which is much higher than the experimental data, which mainly fall in the range of 10^{-5} to 10^{-2}.

This contradict with the condensation trend, described by Park et al [13], that bubble collapses sharply after it reduced to 40% of the initial size. This suggests that bubble would not disappear completely after dropping to 200μm. This suggests that the remnant of the bubble is not water vapor but non-condensable air. Although distilled water is chosen as working fluid, and it had been degassed extensively before the experiments. It cannot guarantee no air trapped in the water. Furthermore, the nucleate boiling on the heated surface relies on the trapped air in the nucleation cavity. Thus, there must be some air trapped in the bubble. This phenomenon was not discussed in literature, might due to two reasons. First, the experimental method can not discern bubble in level of 0.1mm. Thus bubble in this range was discarded. Secondly, the purpose of the experiment was to find the condensation rate, and these tiny air bubbles would not contribute to the heat and mass transfer. Hence, the reducing of condensation rate is neglected in most of the research.

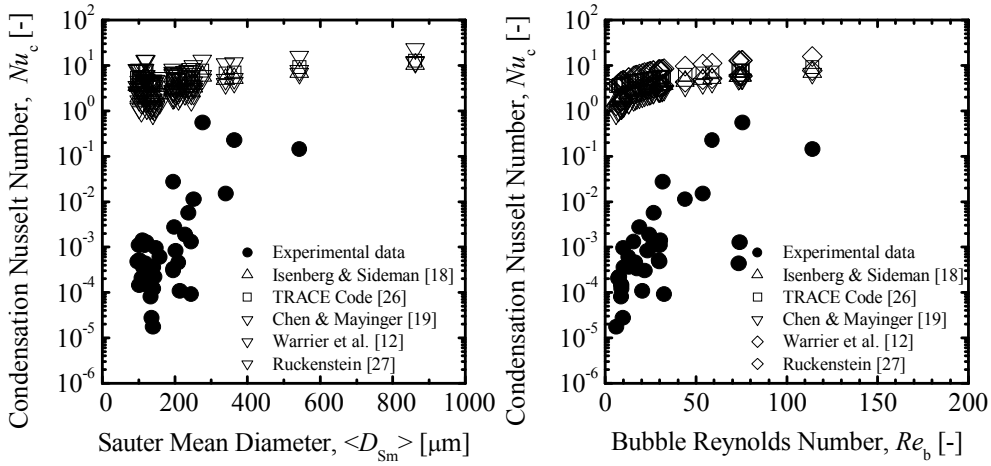

Fig. 5. Bubble condensation Nusselt number.

Table 2. Bubble condensation models.

Author	Condensation Nusselt number	Applicable range
Isenberg and Sideman [18]	$Nu_c = (1/\pi) Re_b^{1/2} Pr^{1/3}$	Non-available
TRACE Code [26]	$Nu_c = 116.7\, Pr^{1/2}$ $Nu_c = 0.185\, Re_b^{0.7} Pr^{1/2}$ $Nu_c = 2 + \left(0.4\, Re_b^{0.5} + 0.06\, Re_b^{2/3}\right) Pr^{0.4}$	$Re_b \geq 10{,}000$ $400 \leq Re_b \leq 10{,}000$ $Re_b \leq 400$
Chen and Mayinger [19]	$Nu_c = 0.6\, Re_b^{0.6} Pr^{0.5}$ (before detachment) $Nu_c = 0.185\, Re_b^{0.7} Pr^{0.5}$ (after detachment)	$Re_b \leq 10{,}000$
Warrier et al. [12]	$Nu_c = 0.6\, Re_b^{0.6} Pr^{1/3} \left[1 - 1.20 Ja^{0.9} Fo_0^{2/3}\right]$	$20 \leq Re_b \leq 700$
Ruckenstein [27]	$Nu_c = \sqrt{4/\pi} \left(Re_b\, Pr\right)^{1/2}$	Non-available

4 Conclusions

Subcooled boiling bubble condensation experiments were conducted in a vertical-upward annular channel by using water as the testing fluid at atmosphere pressure. The test runs comprised of bulk liquid temperatures, velocities and wall heat fluxes ranging from 75.0°C to 98.0°C, 0.25 m/s to 1.0 m/s and 150 kW/m^2 to 200 kW/m^2 respectively. The PDIA system was employed to capture the flow channel at four locations downstream of heated section for a total of 13 test conditions. The bubble Sauter-mean diameter was obtained in the range of 0.1 mm to 0.9 mm. The bubble sizes increase with the increase of liquid temperature or the decrease of liquid velocity. The condensation Nusselt number was calculated to be in the range of 10^{-4} to 10^{-1}, which is much smaller than the typical range of 10^0 to10^2. This might due to the existence of non-condensable gas in the bubble.

References

1. Ishii M and Hibiki T. *Thermo-Fluid Dynamic Theory of Two-Phase Flow*. Elsevier Sciene, 2005.
2. Wu Q, Kim S, Ishii M. One-group interfacial area transport in vertical bubbly flow, *Int. J. Heat Mass Transfer*, Vol. 41, pp 1103–1112, 1998.
3. Hibiki T, Mi Y, Situ R, Ishii M. Interfacial area transport of vertical upward bubbly two-phase flow in an annulus, *Int. J. Heat Mass Transfer*, Vol. 46, pp 4949–4962, 2003.
4. Hibiki T, Ishii M. Two-group interfacial area transport equations at bubbly-to-slug flow transition, *Nucl. Eng. Des.*, Vol. 202, pp 39–76, 2000.
5. Sun X, Kim S, Ishii M, Beus SG. Modeling of bubble coalescence and disintegration in confined upward two-phase flow, *Nucl. Eng. Des.*, Vol. 230, pp 3–26, 2004.
6. Hibiki T, Situ R, Mi Y, Ishii M. Modeling of bubble-layer thickness for formulation of one-dimensional interfacial area transport equation in subcooled boiling two-phase flow, *Int. J. Heat Mass Transfer*, Vol. 46, pp 1409–1423, 2003.
7. Hibiki T, Ishii M. Active nucleation site density in boiling systems, *Int. J. Heat Mass Transfer*, Vol. 46, pp 2587–2601, 2003.
8. Situ R, Mi Y, Ishii M, Mori M. Photographic study of bubble behaviors in forced convection subcooled boiling. *Int. J. Heat Mass Transfer*, Vol. 47, pp 3659–3667, 2004.
9. Situ R, Hibiki T, Ishii M, Mori M. Bubble lift-off size in forced convective subcooled boiling flow. *Int. J. Heat Mass Transfer*, Vol. 48, pp 5536–5548, 2005.
10. Situ R, Ishii M, Hibiki T, Tu JY, Yeoh GH, Mori M. Bubble departure frequency in forced convective subcooled boiling flow. *Int. J. Heat Mass Transfer*, under review, 2006.
11. Zeitoun O, Shoukri M, Chatoorgoon V. Interfacial heat transfer between steam bubbles and subcooled water in vertical upward flow, *ASME J. Heat Transfer*, Vol. 117, pp 402-407, 1995.
12. Warrier GR, Basu N, Dhir VK, Interfacial heat transfer during subcooled flow boiling, *Int. J. Heat Mass Transfer*, Vol. 45, pp 3947-3959, 2002.
13. Park HS, Lee TH, Hibiki T, Baek WP, Ishii M. Modeling of condensation sink term in an interfacial area transport equation, *Int. J. Heat Mass Transfer*, Vol. 50, pp 5041–5053, 2007.
14. Zuber N, The dynamics of vapour bubbles in nonuniform temperature fields, *Int. J. Heat Mass Transfer*, Vol. 2, pp 83-98, 1961.
15. Florschuetz IW, Chao BT. On the mechanics of bubble collapse, *ASME J. Heat Transfer*, Vol. 87, pp 208-220, 1965.
16. Theofanous TG, Biasi L, Isbin HS, Fauske HK. Nonequalibrium bubble collapse: a theoretical study. *Chem Eng. Prog. Sym. Series*, Vol. 66, No. 102, pp 37-47, 1970.
17. Wittke DD, Chao BT, Collapse of vapour bubble with translatory motion, *ASME J. Heat Transfer*, Vol. 89, pp 17-24, 1967.
18. Isenberg J, Sideman S, Direct contact heat transfer with hange of phase: Bubble condensation in immiscible liquids. *Int. J. Heat Mass Transfer*, Vol. 13, pp 997-1011, 1970.
19. Chen YM, Mayinger F, Measurement of heat transfer at phase interface of condensing bubble, *Int. J. Multiphase Flow*, Vol. 18, pp 877-890, 1992.
20. Rayleigh L, On the pressure developed in a liquid during collapse of spherical cavity, *Philosophy Magazine*, Vol. 24, pp 94-98, 1917.
21. Bartel M, Ishii M, Masukawa T, Mi Y, and Situ R. Interfacial area measurements in subcooled flow boiling, *Nucl. Eng. Des.*, Vol. 210, pp 135-155, 2001.
22. Situ R, Hibiki T, Sun X, Mi Y, Ishii M, Flow structure of subcooled boiling flow in an internally heated annulus, *Int. J. Heat Mass Transfer*, Vol. 47, pp 5351-5364, 2004.

23. Whybrew, A., Nicholls, T.R., Boaler, J.J., and Booth, H.J. Diode lasers - a cost effective tool for simultaneous visualisation, sizing and velocity measurements of sprays, *Proceedings ILASS-Europe,* Toulouse, France, 1999.
24. Yule, A.J., Chigier, N.A. and Cox, N.W., Measurement of Particle Sizes in Sprays by the Automated Analysis of Spark Photographs, *Particle Size Analysis*, pp 61-73, London: Heyden Press, 1978.
25. Kashdan, J.T., Shrimpton, J.S. and Whybrew, A. two-phase flow characterization by automated digital image analysis. Part 1: fundamental principles and calibration of the technique. *Particle & Particle System Characterization*, Vol. 20, pp 387-397, 2004.
26. Spore JW, Elson JS, Jolly-Woodruff SJ, Knight TD, Lin JC, Nelson RA, Pasamehmetoglu KO, Steinke RG, Unal C, TRAC-M/FORTRAN 90 (Version3.0) – Theory Manual. *LA-UR-00-910*. Los Alamos National Laboratory, Los Alamos, New Mexico, USA, 2000.
27. Ruckenstein E, On heat transfer between vapor bubbles in motion and the boiling liquid from which they are generated, *Chem. Eng. Sci.*, Vol. 10, pp. 22-30, 1959.

Copyright Statement

The authors confirm that they, and/or their company or institution, hold copyright on all of the original material included in their paper. They also confirm they have obtained permission, from the copyright holder of any third party material included in their paper, to publish it as part of their paper. The authors grant full permission for the publication and distribution of their paper as part of the ISFV13/FLUVISU12 proceedings or as individual off-prints from the proceedings.